Original Paper

Landslides
DOI 10.1007/s10346-021-01837-9
Received: 15 August 2020
Accepted: 16 December 2021

J. A. Gili · R. Ruiz-Carulla · G. Matas · J. Moya · A. Prades · J. Corominas · N. Lantada · M. A. Núñez-Andrés · F. Buill · C. Puig · J. Martínez-Bofill · Ll. Saló · O. Mavrouli

Rockfalls: analysis of the block fragmentation through field experiments

Abstract Fragmentation is a common feature of rockfall that exerts a strong control on the trajectories of the generated blocks, the impact energies, and the runout. In this paper, we present a set of four real-scale rockfall tests aimed at studying the fragmentation of the rocky blocks, from the global design of the field procedure to the data analysis and the main results. A total of 124 limestone, dacite, or granite blocks ranging between 0.2 and 5 m^3 were dropped from different heights (8.5 to 23.6 m) onto four slopes with different shapes (single or double bench) and slope angles (42º to 71º). The characteristics of the blocks, in particular the size, surface texture and joint condition, were measured before the drops. The trajectories of the blocks and both the initial and the impact velocities were tracked and recorded by means of three high-speed video cameras. A total of 200 block-to-ground impacts have been studied. On average, 40% of the blocks broke upon impact on the slope or on the ground, making it necessary to measure the fragments. The initial and final sizes of the blocks/fragments were measured by hand with tape, though photogrammetric techniques (UAV and terrestrial) were also used for comparison purposes. The information gathered during the field tests provides a deep insight into the fragmentation processes. On the one hand, the high-resolution slow-motion videos help to describe when and how the block breakage takes place and the spatial distribution of the pieces. On the other hand, it is possible to compute the block trajectories, the velocities, and the energy losses using videogrammetry. The results include, for instance, a block average fragmentation of 54% and 14% for the limestone and granitoids, respectively; the systematic inventory of the size fragments, which may be used for fitting the power law distributions; and after each breakage, the total angle of aperture occupied by the fragments has been measured, with values in the range 25º–145º. To figure out the different behavior of the blocks in terms of breakage/no breakage, each block-to-ground impact has been characterized with a set of parameters describing the energy level, the robustness of the substrate, and the configuration of the block contact at the impact point, among others. All these terms are combined in a function *F*, which is used to adjust the field data. The adjustment has been carried out, first, for the whole 200 events and later for a subset of them. The procedure and the results are described in the paper. Although the discrimination capability of *F* is moderately satisfactory, it is very sensitive to the test site and setup. It must be highlighted that these field tests are a unique source of data to adjust the parameters of the numerical simulation models in use for rockfall studies and risk mitigation, especially when fragmentation during the propagation is considered.

Keywords Rockfalls · Fragmentation · Real-scale field testing · Rockfall numerical modeling · Landslides

Introduction

Rockfalls are frequent instability processes in road cuts, open pit mines and quarries, steep rock slopes, and subvertical cliffs (Cruden and Varnes 1996; Hungr et al. 2014). Even though the stability of rock slopes can be determined using analytical approaches, the assessment of large rock cliffs requires simplifying assumptions due to the difficulty of working with a large number of joints, the scattering of both the orientations and strength parameters. The attitude and persistence of joints within the rock mass control the size of kinematically unstable rock volumes and determine the way the fragmentation of the detached mass occurs upon impact with the ground surface (Corominas et al. 2017a).

Although there is a transition in the extent of influence from the single block event to the big rock avalanche (Bourrier et al. 2013; Corominas et al. 2018), even small size events can be very destructive due to the high energies and velocities reached during the propagation downslope. The number of yearly casualties is in the same order of magnitude as with other types of slope instabilities (Hoek 2006; Turner and Jayaprakash 2012).

Knowledge of the size and trajectory of the blocks resulting from fragmentation is critical in determining the vulnerability of buildings and protection structures (Jaboyedoff et al. 2005). The probability of occurrence is also necessary for the quantitative risk assessment, QRA (Fell et al. 2005; Corominas et al. 2005; Agliardi et al. 2009; Corominas and Mavrouli 2011; Scavia et al. 2020).

As it is unlikely to witness a real rockfall event, most rockfall inventories concentrate on studying the source point and the spread of the debris over the deposit area, both surveyed well after the occurrence of the event (Abellán et al. 2006; Santana et al. 2012; Ruiz-Carulla et al. 2015, 2016a).

After the detachment, the blocks follow particular trajectories that lead to the final stop point. Several programs are available to model these trajectories, usually considering the individual propagation of blocks. Big improvements have been introduced since the first attempts with a single point falling down a 2D mountain side (see for instance Azimi et al. 1982). The block could be a lumped mass, or it could have a given shape: spherical, cylindrical, or prismatic (Falcetta 1985). The first analyses were in 2D; later, 3D topography was introduced. An overview of the propagation models can be found in Matas et al. (2017). Volkwein et al. (2011) and Ferrari et al. (2016) made extended reviews of qualitative and quantitative methodologies for rockfall hazard assessment.

The fragmentation of the initial detached rock mass is a key aspect both in rock avalanches (Charrière et al. 2015) and in single block events (Giacomini et al. 2009). However, in general, in the

models and methodologies listed so far, the detached rock mass does not fragment during the runout. According to Asteriou and Tsiambaos (2018), the trajectory models have limitations in introducing the fragmentation due to the simplifying assumptions when using the so-called coefficients of restitution (CoR). As a matter of fact, most of the existing propagation models consider the blocks as unbreakable during their propagation (Li and Lan 2015), although there is evidence proving that the rock mass may disaggregate and break after its detachment as a result of the impact with the ground surface, thus producing new rock fragments (Evans and Hungr 1993).

The lack of fragmentation is a simplification that may significantly affect the representativeness of the results (Corominas et al. 2012, 2017a). As shown in Matas et al. (2017), with fragmentation, multiple smaller pieces will diverge from the "average trajectory" of the unbreakable blocks. Eventually, higher bounces and some high-speed pieces (bullets) may be produced (Agliardi and Crosta 2003). This differential performance may significantly change the calculated effect on the inhabitants and the exposed buildings or infrastructure, affecting simultaneously the extent and nature of any remediation measures designed following a QRA analysis. Essentially, when ignoring the fragmentation, the kinetic energy and the runout tend to be overestimated; inversely, the probability of an impact with exposed elements is largely underestimated (Corominas et al. 2012, 2019). Trying to overcome the limitation introduced by the lack of fragmentation, the modeling of individual blocks with sizes similar to those observed in the field is usually carried out (Jaboyedoff et al. 2005; Agliardi and Crosta 2003). Although one can get final spatial distributions similar to the field inventories, the simulated intermediate trajectories and energies may differ from the real ones. Fortunately, in real case studies, when adjusting the results to the field evidence, a good amount of geotechnical and geological judgment, prioritizing the knowledge of the phenomenon and the geomechanical context, can lead to useful results even with limited numerical codes (i.e., 2D models, or codes without fragmentation).

The term "fragmentation" covers the disaggregation of the block pieces delimited by fractures or joints (but sticking together due to a small cohesion or some kind of cementation), and the generation of new pieces, isolated thanks to the creation of new fractures breaking the intact rock itself (Corominas et al. 2012). Undoubtedly, fragmentation is a complex mechanism, conditioned by the previous joints, their persistence (i.e., rock bridges), the energy released, and the angle of each impact relative to the internal rock structure (Zhang et al. 2000; Chau et al. 2002; Wang and Tonon 2011). Due to this complexity, as previously said, the occurrence of fragmentation is rarely considered in current rockfall studies and modeling. Recent research on fragmentation includes empirical as well as analytical works, both in the field and in a model scale. Giacomini et al. (2009), for instance, performed several fragmentation field tests with emphasis on the influence of the impact angle in case of foliated materials; in their work, the number of pieces generated after the block breakage was reported. During field test, it is possible to acquire also the fragment sizes, following, for instance, the methodology shown in Ruiz-Carulla et al. (2015, 2020), and outlined later in the present paper. Haug et al. (2016) did fragmentation experiments in a reduced-scale model with a newly developed rock analogue material. They performed 109 reduced-scale rockslides to study the effect of fragmentation on the average runout and energy balance. On the numerical side, Lisjak et al. (2010) performed the numerical simulation of block fragmentation during propagation using a combined discrete element and finite element method (DEM/FEM), allowing the simulation of multiple interacting bodies and their fragments. Another approach was adopted by Zhao et al. (2016), who used DEM (discrete element method) numerical modeling to simulate the fragmentation of a single prismatic block when it collides with a topographic change of slope; they analyzed the modes of fragmentation depending on the weak or weathered zones of the block.

When trying to introduce fragmentation in our modeling, a further challenge is to characterize the distribution of the resulting fragments. In the literature, for instance, some power law relationships have been proposed for different purposes (Hungr et al. 1999; Dussauge et al. 2003; Corominas et al. 2018); in some cases, the power law is justified with a fractal approach (Ruiz-Carulla et al. 2017). The power law has been successfully used to describe the Young Debris Cover (YDC) after a rockfall event (Ruiz-Carulla et al. 2015, 2016a; Ruiz-Carulla 2018; Ruiz-Carulla and Corominas 2019). Ruiz-Carulla et al. (2020) verified that the power law relationship is also suitable for describing the distribution of the particular pieces after the breakage of a single rock block.

Zhou et al. (2020) used a rockslide real-time video, whereas Asteriou and Tsiambaos (2018) reported a clear fragmentation shot, both incidentally recorded. But, in general, the full event or the block fragmentations upon impact are seldom witnessed in nature. Therefore, it is advisable to carry out real-scale field tests. Rockfall drop tests have been carried out for many years. These are field experiments where rocks are released into a slope to evaluate their trajectories (velocity, height, runout, energy) in order to develop or calibrate numerical models, and, in some cases, to test the performance of rockfall protection measures. In general, blocks are filmed and analyzed with several techniques. An excellent overview of the history of these tests is provided in Duffy and Glover (2017). The so-called "rock rolling tests" have come a long way since Ritchie's (1963) pioneering work, and up until 2017, according to Duffy's estimations, there have been in the order of 15,500 rocks released worldwide in various projects; some campaigns were to calibrate computer models or to determine the degree of hazard associated with rockfall, while others were to test protection measures. In Duffy's words "nothing can replace the value of witnessing a rolling rock impact a barrier and […] watching a rock roll and bound down a slope […] Experience has proven that rolling tests have provided otherwise unknown insights into rockfall behaviour…".

Within rockfall field tests, we can find experiments ranging from low-cost opportunity tests to full-scale setups like Azzoni and de Freitas (1995), Gerber et al. (2001), Dorren et al. (2006), Giacomini et al. (2009), and Spadari et al. (2012), among others. It is worth to mention the well-conducted test included in Bourrier et al. (2021). With few exceptions (Giacomini et al. 2009 for instance), the fragmentation of the blocks has seldom been considered because of the spread that may introduce in the analysis of the results (energy transfer, trajectories of the different pieces, and so on). Gerber et al. (2001) aim to maintain the full energy in an intact block during the barrier testing, whereas Bourrier et al. (2021), in case of fragmentation, keep following the biggest piece of rock for the propagation modeling. In other setups, like Spadari et al. (2012), Caviezel et al.

(2017, 2019), Coombs et al. (2018), Hibert et al. (2019), and Noël et al. (2019), the block breakage is inconvenient because of the presence of accelerometric sensors inside the rock body.

In this context, the R&D projects RockRisk, RockModels, and GeoRisk (Corominas et al. 2017b) aim to improve our knowledge of the rockfall type of rock slope instability. In these projects, a special attention is devoted to the *fragmentation* process and its role in the subsequent rock block trajectories and velocities. The ultimate goal of the projects is to quantify the risk from rockfalls and to develop advanced tools for their study, prevention and mitigation.

The projects include an analysis of the fragmentation laws using data collected from recent and/or controlled rockfall events. In this experimental part of the study, four real-scale rockfall tests were carried out from 2015 to 2017. Once a convenient profile was selected, the test consisted of the release of a number of rock blocks under controlled circumstances. Before, during, and after the fall, a set of parameters and images were recorded. This field work is of paramount importance in order to capture the physical basis of the fragmentation process, to reproduce different features of the fragmentation, the analysis of which can lead to a comprehensive synthesis of the complete phenomenon. On the other hand, the gathered information is useful for adjusting the parameters of the numerical models incorporating the fragmentation.

A description of the first two tests (30 + 26 limestone blocks) together with some preliminary results was reported in Gili et al. (2016) and Ruiz-Carulla et al. (2016b). In the present paper, we are incorporating the third test (44 dacite and granite blocks) and the fourth test (24 limestone blocks). During the series of tests, there has been an evolution in our insight into the fragmentation process and in the technical methods when gathering data in the field (including security issues) and post-processing it. For instance, based on previous experience, the fourth test was specially designed to achieve a higher percentage of block breakage. Therefore, in the first section of the paper, we are now able to give a general description on the drop test organization, which may be useful for the preparation of future experiments dealing with fragmentation studies. Then, we present the main results on the fragmentation gathered in the tests. In the next section, we introduce and discuss the factors that may explain the breakage of the blocks. The paper finishes with a set of concluding remarks.

Test design, site preparation, and test development

When designing a field test, it is important to define the goals of the experiment. For instance, Ritchie (1963) focused on registering the runout of the rocks for highway catchment design; Giacomini et al. (2009) wanted to characterize the impact fragmentation; Gerber et al. (2001) or Giacomini et al. (2012) were centered on the performance of the protection measures; Spadari et al. (2012) focused on the rotational speed/energy of the blocks. The setups and measuring instrumentation were completely different from one case to another.

The four tests reported in the present contribution were mainly oriented to the study of the fragmentation in order to model it adequately within fragmentation algorithms (Ruiz-Carulla et al. 2017; Ruiz-Carulla and Corominas 2019, for instance) and propagation models like RockGIS (Matas et al. 2017 and 2020). Specifically, the objectives of our field tests were:

- direct observation of the fragmentation events and quantification of the percentage of broken blocks.
- acquisition of trajectories $(X, Y, Z)_t$ and their derivatives (velocities and accelerations) in order to measure restitution factors during the impacts block/slope.
- in case of fragmentation: characterization of the envelope of the trajectories of the fragments (aperture).
- in the detention area, inventory of the sizes of the fragments

Due to time and budget constraints, the tests were designed to be low-cost and non-permanent, using the sites only for a few days. For safety reasons, the tests were carried out in quarries, where the blocks were dropped from one bench to the lower esplanade. Although different from natural rockfalls, the geometry of the quarry slopes was favorable for a good acquisition of the impact events at adequate energy levels. The first quarry was a gravel and rockfill open pit located in Vallirana (Barcelona, Spain); both the slopes and the tested rock blocks were limestone. The other quarry (Riudecols, Tarragona, Spain) exploits granitoids for construction and for railway ballast, with a lithology of granite and dacite. As a basic mechanical characterization, limestone has a uniaxial compressive strength of around 103 MPa (estimated from point load tests), a tensile strength (Brazilian test) of around 4.1 MPa, a Young modulus of 119,000 MPa, and an average density of 2650 kg/m^3. The uniaxial compressive strengths for dacite and granite are 159 and 184 MPa, respectively.

The design phase consists of site and profile selection; equipment consideration and setup; and establishment of the procedure for preparing the test, dropping the blocks, and measuring the final scene (including safety guidelines). The explanations that follow are the same for the four tests, although some improvements were introduced over time. We note the tests with a number, 1 to 4, according to the temporal order of realization.

In Fig. 1, the test site profiles are presented. Test 1 is a single-benched slope. Test 2 is a multiple-benched one, although, as will be shown later, the blocks only reached the second bench during the test. Therefore, for analyzing and modeling, this test has only two benches. Test 3, with granitoids, has a high jump, with a first stretch of relatively loose material dipping around 50° and a second part in rock, more vertical. Finally, test 4 site was selected to obtain very energetic impacts at the first contact of the blocks with the slope, against a 42° dip bare rock plane. As can be appreciated in the figure, significant fall heights, including the bulldozer/backhoe blade elevation, range between 8.5 and 23.6 m.

Figure 2 shows the planned equipment and personnel layout around an idealized test. To define the exclusion area for the equipment, a $\beta = 30°$ semi-aperture angle was staked out from the release point(s), right and left from the average dip direction. In doing so, it is important to take into account any change in the dip direction of the slope (as can be appreciated in test 4, Fig. 1a). Similarly, when dealing with the reach distance or runout, we considered a tentative "reach angle" $\alpha = 30°$ (Hungr et al. 2005).

Once the test designed, the list of technical means and supplies was established. These included (Fig. 2): three high-speed video recorders, some additional cameras, a "drone" (or unmanned aerial vehicle, UAV), several staffs and targets (to be used as metric references), a total station, an accelerometer, and a dozer/backhoe

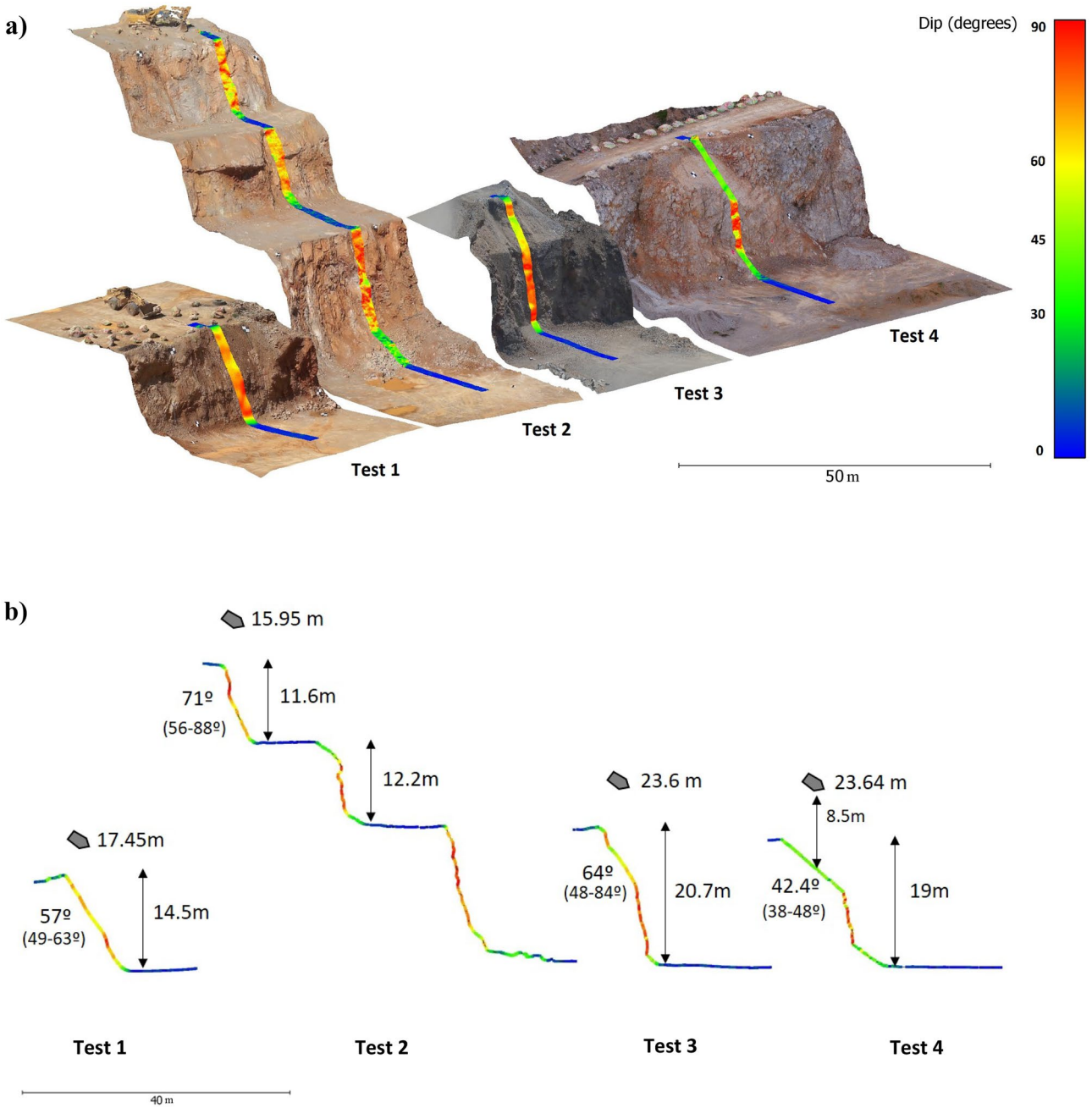

Fig. 1 3D model photo-perspectives (**a**) and profiles (**b**) of the four test sites, with dip values superimposed in color. The gray pentagons symbolize the bulldozer/backhoe blade when releasing the blocks; the average elevation of the blade is indicated. Modified from Ruiz-Carulla et al. (2020)

to carry and release the blocks. The supply of the blocks to test was also arranged, though this was not an issue as the tests were developed in quarries.

After the design phase, the in situ site preparation was carried out. The rolling of the blocks had to be accomplished with a schedule of one day per test due to time and budget constraints. For the four tests reported here, an average of 2–3 people was working on the in situ preparation for 2–3 days before launch day. Most of the site preparation was related with the conditioning of the blocks to be tested. In total, we prepared 132 blocks of massive rock from the same quarry where each test was developed. They ranged between 0.17 and 5.03 m^3, the average being 0.99 m^3, and the mode 1.25 m^3. The final number of tested blocks depended on the actual number of registered fragmentation events and the available time: finally, we dropped 124 blocks in the four tests.

A basic survey was made for each rock block: characteristics of the block, lithology and mineralogical description, joint condition, size, and the Schmidt L hammer rebound, as explained in Gili et al.

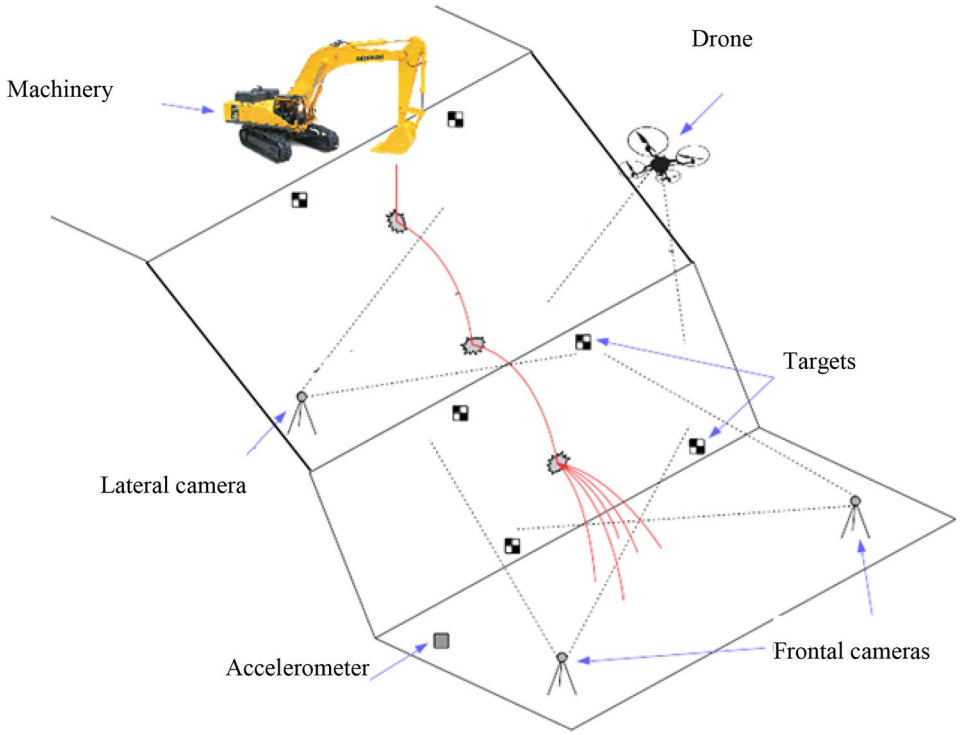

Fig. 2 Perspective sketch with the planned equipment layout for field Tests 1 to 4

(2016). In order to make the blocks more visible during their fall, rotating and bouncing downslope, three major color "circles" were painted over each block surface (Fig. 3a). The detailed geometry (shape and volume) and the surface texture were recorded with a "circular photogrammetric survey" (360°, Fig. 3a). It consists in an enveloping photo report that encircles the block (30 to 60 pictures at different levels), enabling us to build a 3D model of the block (Fig. 3b, c), and to compute the volume, the weight, the gravity center, and the inertia moments (James and Robson 2012). Figure 4 shows several blocks ready for launch on test 1 upper esplanade.

Some additional information about the site preparation can be found in Gili et al. (2016), Ruiz-Carulla et al. (2020), and in the Electronic Supplementary Material (ESM_01.pdf).

The four tests were carried out on 17 June 2015 (test 1), 18 June 2015 (test 2), 8 June 2016 (test 3), and 27 September 2017 (test 4). During the rockfall tests, a minimum of seven people (plus the dozer operator) was necessary to take care of the many systems and duties. Some operations had to be done on the day of the test: positioning the video cameras; setting up the accelerometer; general survey of the area (for the ground control points, GCP, in particular, Fig. 5); and first drone flight. The latter allowed obtaining general 3D models of the slope at each site (Figs. 6 and 1).

An accelerograph (Nanometrics, TitanSMA) was also used during the tests to register the dynamic events in the time domain. The full analysis of the seismic signal falls outside the scope of this paper and has been presented in Saló et al. (2018).

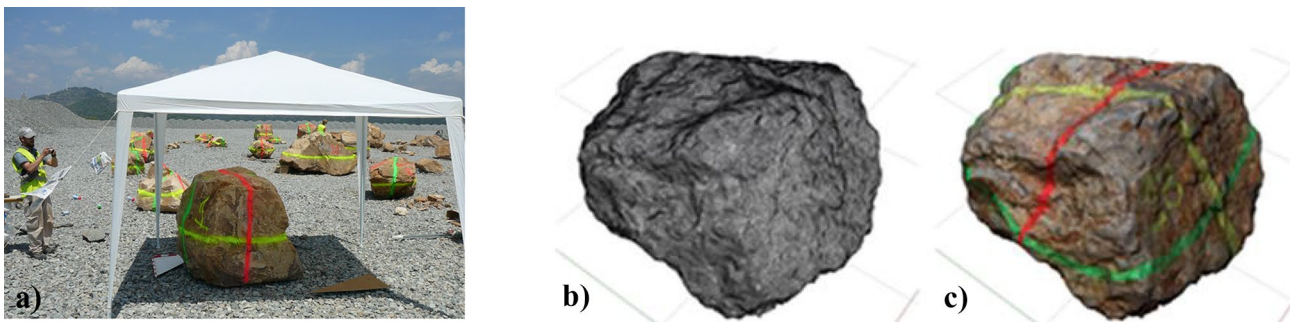

Fig. 3 Block conditioning before the drops, test 3 upper esplanade. Three major color "circles" were painted over each block surface. Then, a 360° photogrammetric survey was carried out (**a**). On the ground, left to the block, note the two red and white 1-m rods used to scale the scene. Examples of the mesh (**b**) and texturized color (**c**) 3D model to be obtained for each block. Each model has around 5 million points, which represent a ground resolution (ground sample distance, GSD) around 2 mm per pixel

Fig. 4 Close view of some limestone blocks ready to be thrown at test 1 site. A big massive one on the left, one with well cemented brecciated limestone in the foreground

Apart from standard picture or video off-the-shelf cameras, the propagation of each block was recorded by means of three high-speed, high-resolution (HS&HR) video cameras that were set up in convergent lines-of-sight (Fig. 2; see the Electronic Supplementary Material, ESM_02.pdf, for characteristics and configuration of cameras).

After the installation of all the cameras and systems, a survey of the different elements (the GCP in particular) was carried out with a reflector-less total station (Fig. 5b) and/or with GPS/GNSS. This was also a good opportunity to make the first drone aerial photogrammetric campaign in order to capture the full scene prior to any damage. During the drop test, the drone was flown several times in order to capture rockfall videos, oblique views (Fig. 5a), and the positions and sizes of the block and the fragments.

As examples of the footage we acquired in the field, Fig. 7 presents a sequence of 4 frames extracted directly from the videos, whereas 3 different times are combined in a single frame in Fig. 8.

Thirty blocks were released at test 1 (single bench); 26 blocks at test 2 (double-benched slope); 44 at Test 3; and 24 at test 4, i.e., 124 drops in total.

After each drop, when the conditions were safe again, an inventory team came in and surveyed the state of the block or the fragments; several pictures were taken as well. In order to characterize the degree and pattern of the fragmentation of the block, the team measured systematically the resulting rock pieces by hand with a tape, assuming either a rectangular or a triangular prismatic shape of the pieces and measuring 3 dimensions of each one. Occasionally, we used other techniques (drone photogrammetry) to measure the volume and position of fragments, but this work is beyond the scope of the present paper. From time to time, the drone was flown over the deposit area. In general, this was followed by fragment removal: the bulldozer cleared the lower esplanade to facilitate the identification of the new incoming blocks/fragments. The frequency for this dozer operation depended on the registered intensity of breakage itself. In the first test (moderate ratio of fragmentation), the area was cleared after every five drops in average, whereas in test 4, where most of the blocks broke, the dozer reconditioned the lower esplanade practically after each drop. The operations referred to in this paragraph (fragment inventory, drone flight, and lower esplanade clearing) were very time-consuming and

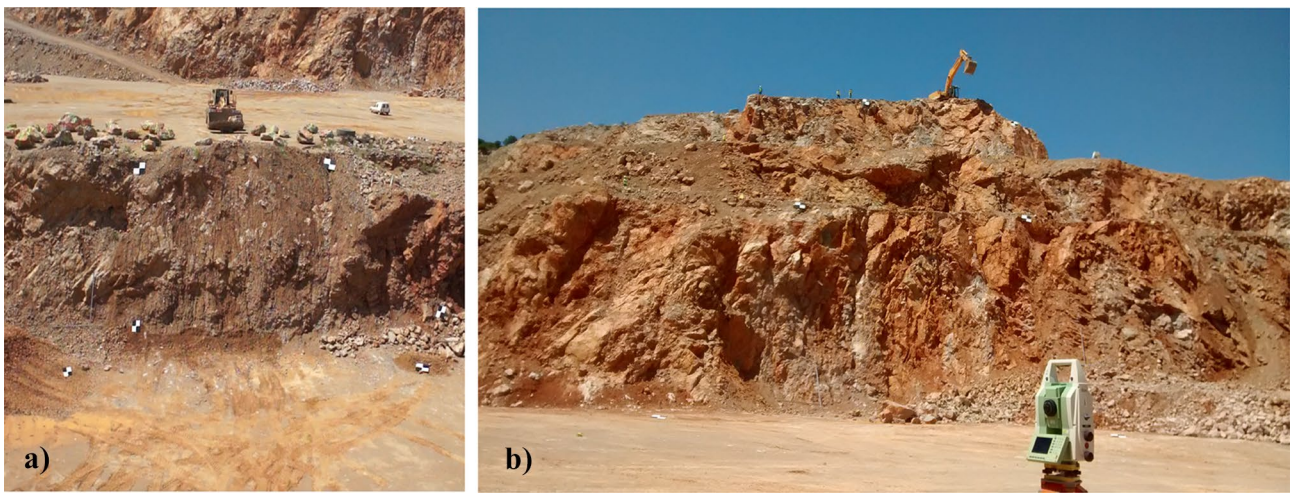

Fig. 5 General view of test 1 (**a**) and test 2 (**b**). Several blocks can be seen left and right of the bulldozer in (**a**). In (**b**) the total station is ready to position the black and white targets used as GCP, which are visible in the pictures

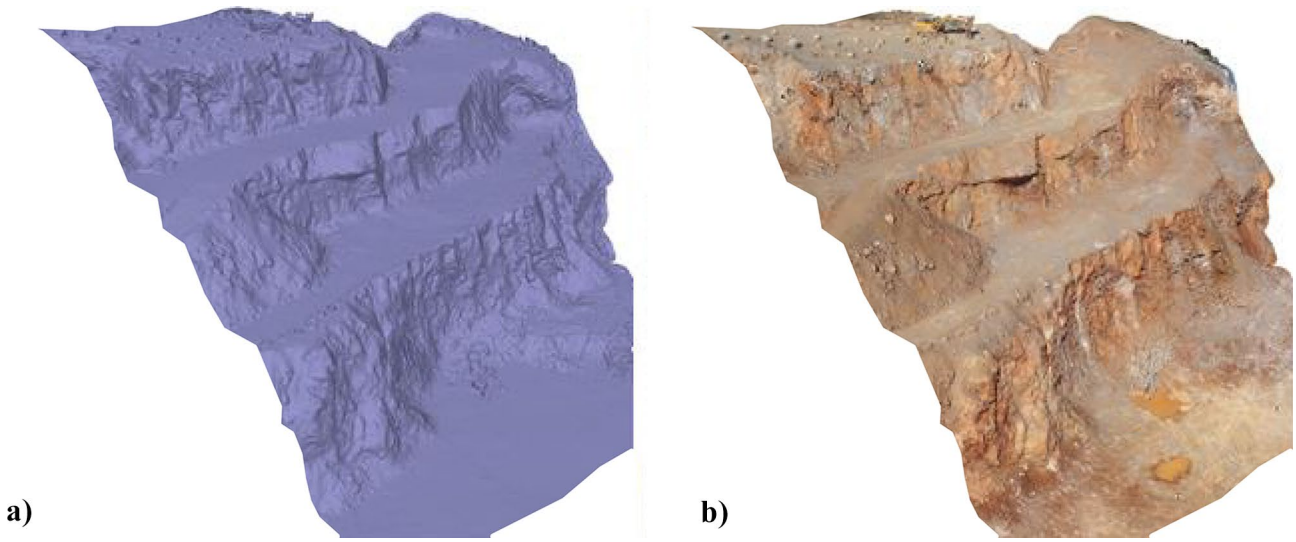

Fig. 6 The 3D model of test 2 site, obtained from the drone flight, is shown shaded (**a**) and color-texturized (**b**). See Fig. 1 to get the scale of the images

laborious; the time investment explains the differences in productivity (number of rolled blocks) among the four tests.

In the Electronic Supplementary Material (ESM_02.pdf), some additional information on the development of the tests can be found. Four example videos are available as well (ESM_03.mp4; ESM_04.mp4; ESM_05.mp4; ESM_06.mp4).

Fragmentation results

In this section, we present the test results, with special emphasis on the characterization of the fragmentation. The field notes and the videos and pictures captured during the four drop tests are the first source of information about the breakage of the blocks and will be summarized in the first subsection. In the next one, we present the angle of aperture of the distribution of fragments after the breakage of the initial block when impacting the ground. This is a particular result that we have been able to extract from the videos acquired during the launches. The results will be discussed in the next section, where we deal with the variability of the behavior of the blocks, working out why some of them break while others remain almost intact.

Field information and data extracted from videos and images

As previously established, the objective of these rockfall tests was to improve our knowledge of the fragmentation processes. Directly during the release of the blocks, or by inspection of the large amount of pictures and videos registered (about 200 GB of files per test), a new insight into the mechanism of breakage of the blocks has been attained. A first observation is that even for the same lithology and falling height, the blocks exhibited a variety of behaviors, ranging from practically no damage to complete shattering (Fig. 9).

Fig. 7 Series with 4 frames extracted from a frontal view video at test 1. This block did not break, globally speaking, although some particles may have become detached from the corners

Fig. 8 Three frames (circled in red) extracted from a lateral shot, combined in a single picture at test 1. This block broke when hitting the lower esplanade

Excerpts of the main results of tests 1 to 4 are presented in a compact form in Tables 1, 2, 3, and 4. Only the first 5 blocks are included; the complete information can be found in the Electronic Supplementary Material (ESM_07.pdf). In each table, the first column contains the number of the block and the second its volume. As more than 60% of the 124 blocks did not break on the first impact with the slope, two impacts can be studied in those drops, increasing the number of impact events to 200 (third and fourth columns in the table). The next four columns correspond to characteristics captured during each particular block impact: the block velocity, the incidence angle, the substrate type, and the impact morphology. The exact meaning of these parameters will be fully developed and discussed in the following subsections, similarly with the next two columns, related with the kinetic energy. Finally, the last column contains an overall assessment of the block performance with respect to the fragmentation: one (1) means that the block was "significantly fragmented", and zero (0) means that the block survived. By "significantly fragmented", we mean the breakage of an important fraction of the block (Fig. 9b to d) and exclude the cases in which some small particles may have fallen off the corners of the block (Fig. 9a).

The first overall result of Tables 1–4 may be, for instance, the global percentage of "significantly fragmented" blocks during the tests: it can be established as 39.8% globally for the four sites. Grouping the drops by lithology, we get an average of 53.8% of breakage for limestone (tests 1, 2, and 4), and 14% for granitoids (dacite and granite, test 3). These values must be prudently considered because they are completely site-dependent. For instance, for the limestone blocks the percentage ranges between 41.1 (tests 1 and 2) and 83.3% (test 4). Some insights for explaining this variability will be developed later in this section. Nevertheless, the 39.8% of breakages has been considered satisfactory under the objectives of the research projects mentioned before, because we have a spread of intact block trajectories combined with fragmentation events.

The videos recorded during the tests allowed us to identify the fragmentation instant (Fig. 10) and to follow the disassembly of the original block into pieces that pull apart carrying different energies and velocities (Figs. 8, 11, 12a). The direct examination of the impacts in the different convergent videos permitted the assessment of the parameters *"terr_imp"* and *"geom_imp"* (Tables 1–4). On the other hand, the videotriangulation (Fig. 12) served to measure the velocities and the incidence angle of the blocks upon impact on the slope wall and on the esplanade (columns v_i, γ_i, in Tables 1–4). The use of the videos for the extraction of the aperture angle upon breakage is shown in the next subsection. Details on the videogrammetry processing can be found in Prades et al. (2017).

In the Electronic Supplementary Material (ESM_08.mp4), some shots including fragmentation events have been merged to exemplify the extraction of information from the high-speed video material.

In Fig. 13, an overview of the behavior of the 124 blocks dropped in tests 1, 2, 3, and 4 is presented, with the number of inventoried fragments (594, 680, 392, and 1241, respectively). By dividing it by the number of released blocks per test site, we obtain the average number of inventoried fragments per block (also called multiplier factor, MF). The graphs show clearly that test 3 (dacite and granite) registered fewer breakages (MF around 9), while Test 4 was the most "successful" (MF around 52).

After a block breakage, the size of the fragments can be characterized by means of power-law relationships used to adjust field results. A full description of these size distributions can be found in Ruiz-Carulla et al. (2020). The exponents range between 0.31 and 0.54.

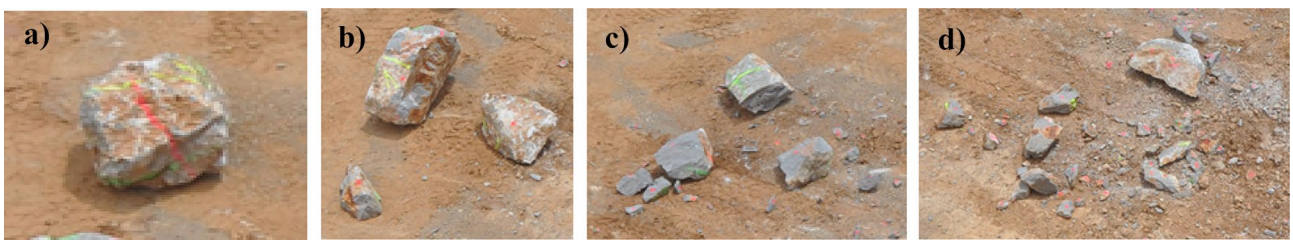

Fig. 9 Different block behavior during the tests. (**a**) Practically intact; (**b**) breakage into a few pieces; (**c**) block splits into several well-defined pieces; (**d**) intense breakage and shattering. These examples are taken from limestone tests, the size of the original blocks range between 0.5 and 1 m^3

Table 1 Excerpt of test 1 main results (single bench, limestone)

Measured before drop		Determined during the drop						Computed from previous		Overall performance
#Block (-)	Volume, V (m^3)	Event number	#Impact (slope or esplanade)	v_i (m/s)	γ_i (°)	*terr_imp* (-)	*geom_imp* (-)	E_{kin} (KJ)	E^*_{kin}/m (m^2/s^2)	F(1)/NF(0) (-)
1	1.25	1	1 (slope)	13.8	15.0	3.5	1	315.4	6.4	0
		2	2 (esplanade)	15.2	80.0	3.5	3	383.7	112.3	1
2	0.85	3	1 (slope)	13.1	20.0	4	1	193.3	10.0	0
		4	2 (esplanade)	14.3	85.0	3	3	230.3	101.5	1
3	0.82	5	1 (slope)	10.5	26.0	4	3	119.8	10.6	0
		6	2 (esplanade)	14.5	58.7	4	1.5	229.4	77.1	1
4	1.18	7	1 (slope)	11.8	21.0	4	2	217.7	8.9	0
		8	2 (esplanade)	14.3	53.1	3	1	321.1	65.7	0
5	1.91	9	1 (slope)	11.8	19.0	4	2	352.4	7.4	0
		10	2 (esplanade)	14.8	53.9	2	1.5	554.3	71.5	0

v_i block velocity just before the impact

γ_i incidence angle, relative to the terrain slope (Fig. 14)

terr_imp, *geom_imp*, E_{kin}, E^*_{kin}/m see explanations in the text (Tables 6–8)

Only 5 out of 30 drops are shown here

Angle of aperture of the trajectories after the breakage

When a block breakage is registered, in addition to the number and volume of the resulting pieces, it is also interesting to estimate their directions and velocities. In Matas et al. (2017), the Fig. 14 approximation is adopted. Some of the breakage events registered during the four tests were suitable for measuring the angle of aperture of the trajectories, θ. Figure 15 presents two examples of the direct extraction of θ from the videos. The measured values range between 25° and 145°, with an average value of 75° (Matas et al. 2020).

Discussion on the factors affecting the breakage of blocks

In this section, we deal with the variability in the behavior of the blocks, working out why some of them break, while others remain almost intact. The variability (Fig. 13) is notable but nothing unusual for natural materials and real tests (Gerber and Caviezel 2017, for instance). Most of the tested blocks were massive although some of them displayed a variable number of finite fissures, partly cemented (Fig. 4). On the other hand, some clear candidates for breakage remained unbroken (Fig. 16). Looking at the characteristics of the rock blocks before and after the tests, one may wonder if it is possible to elucidate the reason for the different behavior. The challenge is to explain why some blocks break into several fragments, while others that impact with a similar energy level remain almost intact.

To explain the breakage/non-breakage behavior, some physical reasons must exist, related with the geometry and mechanics during the impact. A list of parameters influencing the rock rebound is summarized in Asteriou et al. (2012), Asteriou and Tsiambaos (2016), and Labiouse and Heidenreich (2009). Among them, we wish to highlight the seven "parameters" (or grouped factors) listed in Table 5.

The first argument to explain the breakage should be the investigation of the kinetic energy during the impact (*i* and *ii* in Table 5). The videogrammetry permitted the computation of the kinematics of the blocks on the main impact point (translational velocity v_i reflected in Tables 1–4). The measured velocities on the first impact (slope) are in good correspondence with the free fall speed from the release point height. The block volume (V, Tables 1–4) and the average density (presented in Test design, site preparation & test development) permit the computation of the block mass, m, and the translational *kinetic energy* (E_{kin} in Tables 1–4):

$$E_{kin} = \frac{1}{2} m v_i^2 \quad (1)$$

The rotational energy may play a role in some cases (Volkwein et al. 2017). Although the rotational velocity can be measured from the HS videos, it is not straightforward (Prades et al. 2017). Some rough checks into our drops permitted us to assess that, in general, the rotational part reaches only a small fraction (less than 15%) of the total kinetic energy. While the rotational energy might be considered in the future following the works of Prades et al. (2017), its contribution and role have been disregarded here.

In Gili et al. (2016), we presented some preliminary plots exploring the relationship between the kinetic energy and the fragmentation of the blocks in test 1 and test 2. Those graphs showed a clear

Table 2 Excerpt of test 2 main results (double-benched slope, limestone)

Measured before drop		Determined during the drop						Computed from previous		Overall performance
#Block (-)	Volume, V (m^3)	Event number	#Impact (slope or esplanade)	v_i (m/s)	γ_i (°)	*terr_imp* (-)	*geom_imp* (-)	E_{kin} (KJ)	E^*_{kin}/m (m^2/s^2)	F(1)/NF(0) (-)
1	0.39	60	1 (slope)	10.0	25.0	4	1	51.3	8.9	0
2	0.35	61	1 (slope)	9.8	26.3	4	2	43.9	9.4	0
		62	2 (esplanade)	16.9	80.0	3	3	130.6	138.5	1
3	0.33	63	1 (slope)	9.5	26.0	4	1	39.3	8.7	0
4	0.32	64	1 (slope)	9.3	24.9	4	1.5	36.2	7.6	0
5	0.56	65	1 (slope)	10.5	27.0	4	3	81.4	11.4	0
		66	2 (slope)	8.3	20.6	4	1	51.5	4.3	1

Only 5 out of 26 drops are shown here

Table 3 Excerpt of test 3 main results (granitoid quarry)

Measured before drop		Determined during the drop						Computed from previous		Overall performance
#Block (-)	Volume, V (m^3)	Event number	#Impact (slope or esplanade)	v_i (m/s)	γ_i (°)	*terr_imp* (-)	*geom_imp* (-)	E_{kin} (KJ)	E^*_{kin}/m (m^2/s^2)	F(1)/NF(0) (-)
1	1.32	90	1 (slope)	9.4	30.0	1	2	154.5	11.0	0
		91	2 (esplanade)	17.6	55.9	2.5	1.5	541.8	106.4	0
2	0.75	92	1 (slope)	9.6	37.0	1	2	91.6	16.7	0
		93	2 (esplanade)	18.7	66.3	2.5	2	347.5	146.6	0
3	0.42	94	1 (slope)	9.9	32.0	1	1.5	54.4	13.8	0
		95	2 (esplanade)	17.3	69.8	2.5	1	166.2	131.8	0
4	0.61	96	1 (slope)	10.7	34.0	1	1	93.0	17.9	0
		97	2 (esplanade)	18.1	72.1	2.5	3	265.5	148.0	0
5	0.40	98	1 (slope)	9.7	37.0	1	2	49.4	17.0	0
		99	2 (esplanade)	17.9	69.7	2	1	168.5	141.2	0

Only 5 out of 44 drops are shown here

Table 4 Excerpt of test 4 main results (limestone, 42° bare rock plane)

Measured before drop		Determined during the drop						Computed from previous		Overall performance
#Block (-)	Volume, V (m^3)	Event number	#Impact (slope or esplanade)	v_i (m/s)	γ_i (°)	*terr_imp* (-)	*geom_imp* (-)	E_{kin} (KJ)	E^*_{kin}/m (m^2/s^2)	F(1)/NF(0) (-)
1	0.68	175	1 (slope)	10.6	47.6	4	1.5	100.9	30.6	1
2	1.36	176	1 (slope)	10.7	47.1	4	2	205.6	30.7	1
3	1.23	177	1 (slope)	11.4	48.1	4	3	210.4	35.8	1
4	0.71	178	1 (slope)	12.5	47.6	4	2	147.2	42.7	0
		179	2 (esplanade)	15.9	82.0	2.5	1	237.8	124.0	0
5	1.55	180	1 (slope)	9.9	46.0	4	1	201.6	25.4	1

Only 5 out of 24 drops are shown here

lack of correlation between the translational *kinetic energy* (E_{kin}) and the fragmentation. It seems that the breakage/non-breakage occurrence did not depend only on the absolute level of the energy present during a given impact. In the aforementioned contribution, we were unable to identify an energy threshold separating the breakage/non-breakage behavior (similarly with Giacomini et al. 2009). It is worth mentioning that our tests were not specifically designed to identify this hypothetical threshold, as the range of energies was not wide enough (20–1944 kJ, see Tables 1–4).

However, even with this narrow range of energies, some blocks remained intact, while others broke into numerous pieces. For instance, for test 1, we realized that the most energetic impact (1228 kJ, drop 23) failed to break the block. Actually, this was the biggest block, around 4.6 m^3. One may wonder whether the correlation will appear if we use the "specific" translational kinetic energy of the blocks (the translational kinetic energy per unit of mass), i.e.:

$$E_{kin}/m = \frac{1}{2}mv_i^2/m = \frac{1}{2}v_i^2 \tag{2}$$

When plotting this value against the fragmentation, again, no clear trend, correlation, or threshold appears, probably because what really matters is the amount of energy *normal* to the slope at the impact point, which depends on the attitude trajectory/slope.

Actually, the next influencing parameter (*iii* in Table 5) is the angle of the trajectory when the block impacts the ground (incidence angle, γ_i, Fig. 14). This incidence angle (Tables 1–4) was different in each impact and was derived from the HS&HR videos, by videogrammetry.

The component of the velocity *normal* to the face (v_n) is:

$$v_n = v_i \sin\gamma_i \tag{3}$$

Thus, the translational kinetic normal energy per unit of mass (named *specific normal energy*, E^*_{kin}/m in Tables 1–4) is:

$$E^*_{kin}/m = \frac{1}{2}v_i^2 \sin^2\gamma_i \tag{4}$$

When we plotted this *specific normal energy* against the fragmentation, a slight trend was appreciated, which is indicative that this energy parameter may be significant in order to explain the block breakage, but only to a certain extent.

Examining the *specific normal energy* levels per lithology, the average in the limestone tests (tests 1, 2, and 4) is 43 m^2/s^2; they exhibited a 53.8% of significant breakage. On the other hand, in test 3 (granitoids) with a higher *specific normal energy* level (60 m^2/s^2), we experienced a markedly lower degree of breakage (14%). The importance of the lithology is beyond any doubt, and that is why it is considered in Table 5 (line *vii*).

Comparing only the limestone tests, we realized that, with a similar level of *specific normal energy*, the percentage of fragmentation events in test 4 is roughly double the percentage of tests 1 and 2. We must conclude that there are other important parameters, not included in our analysis so far, which may help to explain the fragmentation/no fragmentation behavior of the blocks.

In Table 5, the fourth and fifth influencing factors are somehow related: the nature of the ground where the impact takes place, and the average deformability of the contact block-ground. During the field tests, we realized the paramount importance of these

Fig. 10 Frame corresponding to the breakage instant (block 2, test 4, drone nadiral view). The fragmentation of the original block can be clearly appreciated

two aspects, related with the substrate strength and its absorbing or damping effect upon the block rebound. Depending on the substrate where the block contacts the slope or the esplanade, the energy is dissipated, or, alternatively, recovered in a high percentage and maintained inside the propagation phenomena. If a block hits a plane of bare bedrock, or a layer of rock scree, or soil fill, the overall performance is very different, both in terms of the trajectory and in terms of the possible fragmentation. In order to incorporate this important feature in the analysis, we created a parameter to assess the substrate type at the impact point, named "*terr_imp*", which has been established through field reconnaissance complemented with observation of the different HS&HR videos, drop by drop. The subjective criteria to assign the value "*terr_imp*" to each impact are detailed in Table 6, and the values estimated for each impact are listed in Tables 1–4.

Following the identification of parameters influencing the performance of the blocks, the sixth one in Table 5 introduces the role of the configuration of the impact. This factor is mostly random during a given block propagation: the block may contact the ground with a full face, or, alternatively, only with an edge/corner. Fortunately, in our tests, it has been possible to determine the contact mode of the majority of impacts by means of the HS&HR videos.

Fig. 11 Semi-automatic extraction of the trajectory of the original block and some of the fractions by videogrammetry (block 3, test 1, multi-frame composition, lateral high-speed camera)

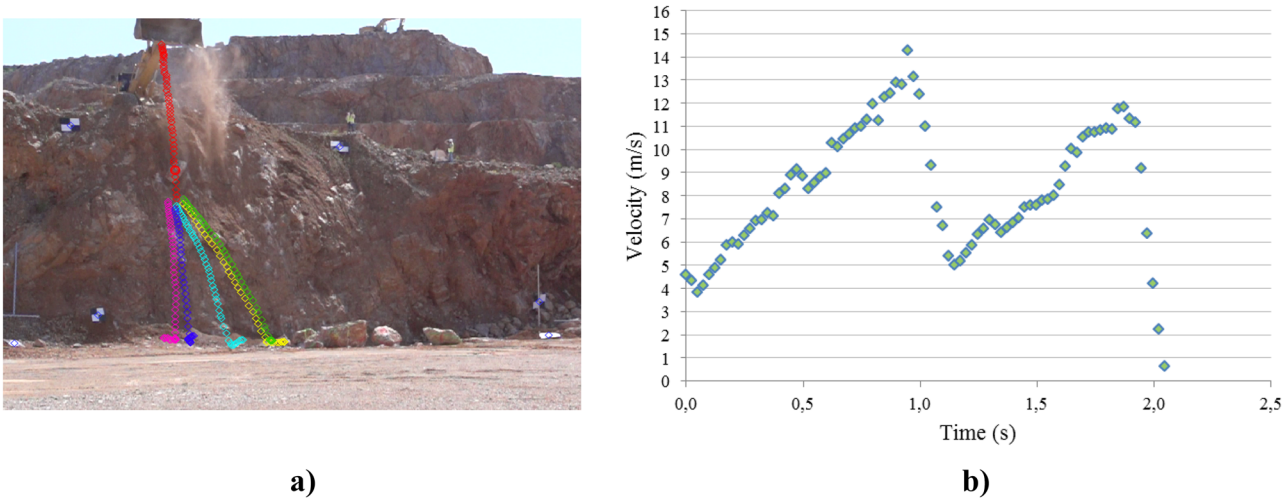

Fig. 12 (**a**) example of trajectories from semi-automatic videotriangulation (Prades et al. 2017), block 19, test 1. (**b**) Velocity vs. time. The acceleration periods and the energy losses during the impacts can be clearly identified

To quantify the impact morphology, we created a new parameter named "*geom_imp*", which is determined according to the criteria shown in Table 7 and listed in Tables 1–4.

The last influencing parameter to consider (Table 5) is the seventh, which encloses the internal structure of the block: the number and spacing of the joints, persistence (rock bridges), fill, and cementation. These characteristics determine the overall block strength against breaking on impact. It is very difficult to characterize, even indirectly, all these features. As explained in Test design, site preparation & test development, our first attempt was using the L hammer (systematic measurements of the surface Schmidt hardness). A similar sclerometer was used, for instance, by Matthews et al. (2018) (surface degradation of boulder deposits under aging) and Asteriou and Tsiambaos (2018) (to characterize small, uniform, spherical particles). However, in our tests, when trying to correlate the rebound and the fragmentation/non-fragmentation behavior of the real blocks, the results showed a lack of correlation (Gili et al. 2016). This kind of technique characterizes only the immediate centimeters close to the sclerometer impact point, being absolutely insufficient to represent the average state of the block, its fissuration and its resilience against disintegration.

To overcome the limited penetration of the L hammer, in field test 3, we characterized some blocks with an ultrasonic sclerometer, Pundit type, 50 kHz, following the laboratory works of Moradian and Behnia (2009) and Yasar and Erdogan (2004). We found that the measured propagation speeds were sensitive to the internal structure of the blocks (existence of joints, aperture, and cementation/fill) as intended. However, the measurement process (several scanlines per block) was laborious in field conditions. We were able to survey a limited number of blocks (fifteen blocks in Test site 3). For these fifteen cases, we translate the sclerometer measurements (several scanlines crossing the block) to a parameter estimating the average block quality, named "*i_pundit*", defined in Table 8. Some details on how the ultrasonic sclerometer was used (ESM_01.pdf), along with the values of the "*i_pundit*" parameter for each block (ESM_07.pdf), can be found in the Electronic Supplementary Material. Despite the aforementioned limitations, we consider that this geophysical method is promising for the characterization of blocks prior to their release.

Summarizing this section so far, in an attempt to explain why some blocks break while others do not, we have translated the group of seven parameters influencing the block performance (Table 5) into some factors that can be derived from the data gathered during our drop tests:

- Specific energy ($½ \cdot v_i^2$) and incidence angle (γ_i), which merge in the *specific normal energy* value
- Substrate at the impact point ("*terr_imp*")
- Morphology of the impact ("*geom_imp*")
- The internal structure (joints, persistence, strength) of the block ("*i_pundit*")
- The lithology

When one tries to study the correlation of these factors, one by one, with the breakage event (F/NF column in Tables 1–4), the results are quite scattered, indicating that we must consider all the factors simultaneously in order to explain the overall performance of the block. One way to achieve this is to design a *function or operator* working with the basic information for each block/impact.

In the present contribution, we are trying to explain the test results adequately. We are not proposing a new "geomechanical classification for block fragmentation tests", but the concept of "geomechanical classification" may be useful in the sense that it assesses complex geomechanical situations based on simple parameters. These are sometimes evaluated in a partially subjective manner due to the limited nature of the data. When working with RMR (Bieniawski 1993), Q (Barton et al. 1974), SMR (Romana et al. 2003), and even with the GSI (Marinos and Hoek 2000), one accepts that these classifications give an average expected general behavior instead of an exact computation or a likely, infallible prognosis.

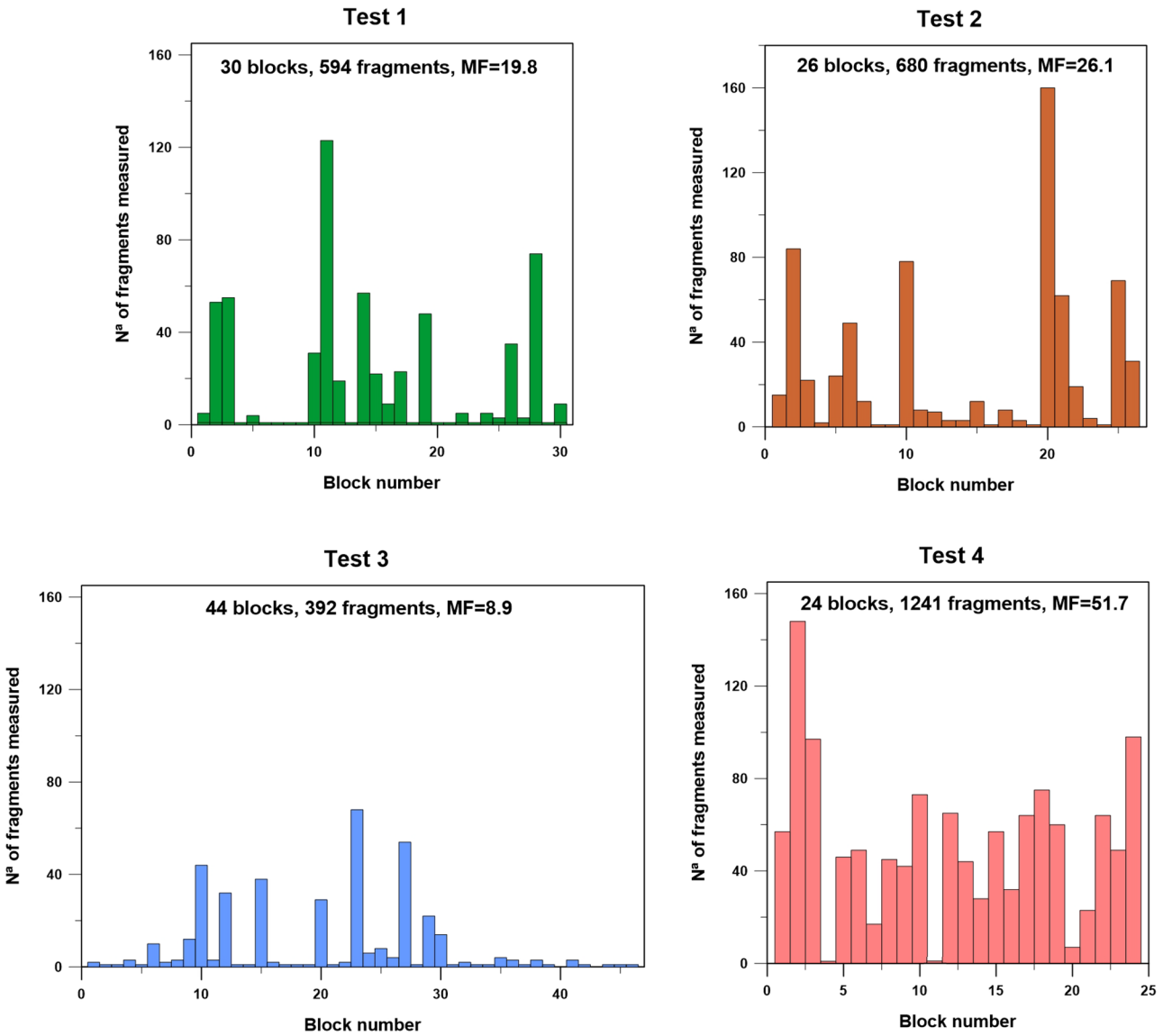

Fig. 13 For tests 1 to 4, the number of fragments inventoried on the esplanade after the release of each block. $N=1$ means that the block remained intact after the drop. MF, or multiplier factor, is the average number of inventoried fragments per block

After several trial and error attempts, we propose a *functional*, F (Eq. 5), using the ideas underlying the principles of multivariate analysis. As the breakage event is a simultaneous occurrence of some favorable circumstances (altered block *and* stiff ground *and* high energy *and*…), the proposed *functional* is a multiplication of a number of terms:

$$F = \left[\frac{V - V_0}{V}\right]^a \cdot \left[1 - \frac{\sigma_c}{2{\cdot}\sigma_{max}}\right]^b \cdot \left[\frac{E^*_{kin}/m}{SNE_{max}}\right]^c \cdot \left[\frac{terr\_imp}{4}\right]^d \cdot \left[\frac{geom\_imp}{3}\right]^e \cdot \left[\frac{i\_pundit}{4}\right]^f \quad (5)$$

each multiplier will range between 0 and 1, as will their product. So F will also span the interval [0, 1]. According to the proposed methodology, if F approaches 0, the block will remain intact, whereas if F approaches 1, the block will break (on average). An explanation of the different terms follows.

As seen in the equation, each influencing variable is enclosed in a multiplier or term, affected by an exponent. The expressions in the brackets have been designed to range between 0 and 1. The exponents (a, b, c, d, e, f) should be positive and account for the possible non-linearity between each term and the overall F. Therefore,

a. Volume term: It takes into account the influence of the volume V (size or mass) of the block. For the same rock mass, a big block will intersect more and more discontinuities, being, in principle, more prone to breakage. V_o is some kind of irreducible volume. When V approaches V_o, the block tends to be unbreakable. For

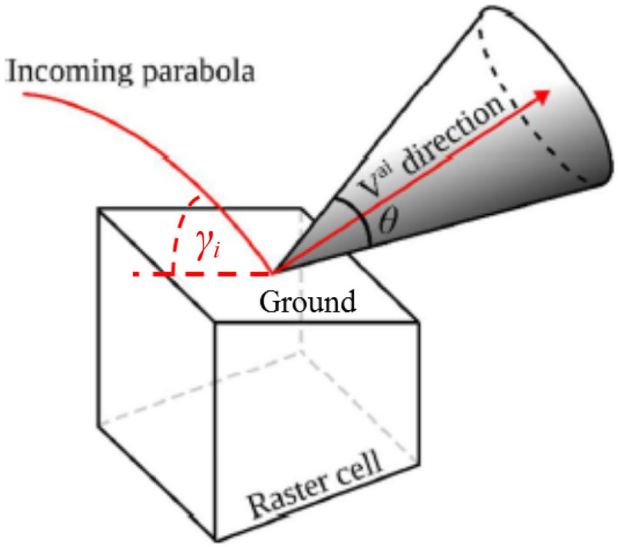

Fig. 14 Simplified approach adopted in Matas et al. (2017) for the angle of aperture: the trajectories are stochastically distributed in a cone with a total angle of aperture θ, and with an axis in the direction of the computed velocity after the impact, V^{ai}

a very big volume, this term will approach 1; this means that the breakage of the block will depend completely on the remaining terms.

b. Lithology term: It accounts for the compressive strength (σ_c) of the intact rock composing the block. σ_{max} is the biggest σ_c in the analysis. We introduced a 2 in the denominator to get an overall value of 0.5 when $\sigma_c = \sigma_{max}$, the decay being controlled by the exponent, b.

c. Energy term: The numerator of this term is the *specific normal energy* as discussed above in this section. SNE_{max} is the maximum value of this energy in the data set.

d, e, f terms: Based on the "*terr_imp*", "*geom_imp*", and "*i_pundit*" values discussed above in this section, these three expressions introduce the importance of the substrate where the block impacts, the configuration of block upon impact (edge, corner, face) and the internal structure of the block, respectively.

For a given set of tests, F must be adjusted to the experimental data by working out the set of exponents (a to f) that better match the observed global performance, F/NF. These exponents control the non-linear contribution of each term to F. They must be regarded more as mathematical tools than as weights of the different terms. In order to limit the search and the non-linearity of F, the exponents have been constrained to an interval of 0.25 to 4.

The expression for F can also be used with missing or incomplete information. One can substitute the term with no data by an average value. Or, if there is no data for a term for all the blocks, the term can be taken out of the adjustment. Undoubtedly, the final aspect of function F will depend on the set of data used for its adjustment. But, once determined, the function will be useful to discriminate F/NF behaviors.

For the tests presented in this paper, the adjustment of F was carried out for two sets of cases. Firstly, the whole 200 events in Tables 1–4 are used. Secondly, only the subset of events having an assessment of the *i_pundit* term was used for a separated F adjustment.

First adjustment

For the adjustment of the 200 impact events, we disregarded the first, the second, and the last terms of the F full expression (Eq. 5) for the following reasons. In our tests, the block volumes were much bigger than any V_o one can envisage; as the volume term was always very close to the unity, we pushed it aside for the sake of simplicity. On the other hand, we got the strength (σ_c) only as an average per lithology, not block per block. The homogeneous value of the lithology term does not help in the task of discriminating the behavior of the different blocks, so we dismissed it. As previously said, the last term ("*i_pundit*") was available only for part of the sample; thus, it has been disregarded.

So, three terms have been considered in the F adjustment for the 200 events shown in Tables 1–4, with the best-fit resulting exponents as follows:

- $c = 0.29$ for the energy term
- $d = 3.77$ for the substrate type term
- $e = 0.25$ for the impact morphology term

Fig. 15 In red, envelope cones adjusted to two breakage events, test 1. (**a**) Block 19, the breakage happened on the slope ($\theta \approx 33^o$). (**b**) Block 2, the breakage happened on the esplanade ($\theta \approx 100^o$)

Fig. 16 Two limestone blocks that remained unbroken after the drop, although they exhibited some karstic dissolution features, partially cemented

Thus, F adopts this form:

$$F = \left[\frac{E^*_{kin}/m}{SNE_{max}}\right]^{0.29} \cdot \left[\frac{terr\_imp}{4}\right]^{3.77} \cdot \left[\frac{geom\_imp}{3}\right]^{0.25} \quad (6)$$

This tentative expression permitted a preliminary assessment of the capability of function F to explain the breakage/non-breakage behavior of the blocks during Tests 1–4. In Fig. 17, the F value computed for each block according to Eq. 6 (horizontal axis) is compared with its actual behavior (vertical axis: 1 – fragmentation –, 0 – no fragmentation –, last column in Tables 1–4). Although some points are misclassified by the approach (highlighted in red), at last, considering simultaneously the different influencing parameters at play, some adequate trend has been obtained.

The vertical dashed green line, $F = 0.428$, is a threshold value to discriminate, in average, the blocks in the "break/no-break" aspect. To reach this value, tentatively, we moved the vertical line to the position where it let the same number of misclassified points to its left and to its right (FN and FP, respectively, Fig. 17). If we use the "Accuracy", (TP + TN)/(TP + FP + FN + TN), to measure the overall "performance of the function F when classifying the block behavior", we get (35 + 136)/(35 + 14 + 15 + 136) = 85.5%

Table 5 Parameters influencing the block performance during the impact with ground (modified from Asteriou and Tsiambaos 2016)

i	Mass and shape of the block
ii	Translational and rotational block velocities
iii	Incidence or collision angle of the block trajectory on the ground
iv	Nature of the ground where the impact takes place: bare bedrock, rock scree, soil fill
v	Average deformability (stiffness) of the block part contacting the slope
vi	Configuration of the block upon impact (e.g., which part of it contacts the ground: face, edge, corner)
vii	Internal structure of the block, (related with its strength, lithology, fissuration)

Table 6 Criteria to assign the value "*terr_imp*" (substrate type at the impact point)

"*terr_imp*"	*Description*
1	A thick layer of soil or gravel (rock pebbles) covers the surface at the impact point
2	A medium layer of soil or gravel covers the surface at the impact point
3	A thin layer of soil or gravel covers the surface at the impact point. There is rock-to-rock contact
4	Bare bedrock. There is rock-to-rock contact. Clear rebound in case of no block breakage

An extended version of this table can be found in the Electronic Supplementary Material (ESM_09.pdf)

Table 7 Criteria to assign the value "*geom_imp*" (morphology of the impact)

"*geom_imp*"	*Description*
1	The block hits the ground with an edge contacting it
2	The block hits the ground with a vertex or corner contacting it
3	The block hits the ground with a full face contacting it
–	Undefined (doubtful cases where the video footage was not clear enough)

Table 8 Criteria to assign the value "*i_pundit*" (internal block structure from ultrasonic measurements)

"i_pundit"	*Description*
1	Strong, massive, unlikely to break. The signal crosses the block for all the scanlines
2	Less massive. The signal crosses the block for almost all the scanlines
3	Medium weak. The signal crosses the block for less than half of the scanlines
4	Weak block, might break at first impact. No or few successful scanlines

Second adjustment

This adjustment was carried out with a subset of cases: only the events having an assessment of the "*i_pundit*", i.e., 30 impact events corresponding to the 15 blocks in test 3 whose "quality" was indirectly established with the Pundit sclerometer. As the "*i_pundit*" value was introduced in the adjustment, we had four terms and their respective exponents. The best-fit results were:

- $c = 1.37$ for the energy term
- $d = 4.00$ for the substrate type term
- $e = 0.25$ for the impact morphology term
- $f = 0.26$ for the block quality term

So, in this case, the function F will look like this:

$$F = \left[\frac{E^*_{kin}/m}{SNE_{max}}\right]^{1.37} \cdot \left[\frac{terr\_imp}{4}\right]^{4.00} \cdot \left[\frac{geom\_imp}{3}\right]^{0.25} \cdot \left[\frac{i\_pundit}{4}\right]^{0.26} \quad (7)$$

Note the difference in the corresponding exponents when compared with the first adjustment.

In Fig. 18, the predicted breakage/non-breakage behavior of the blocks is compared with the real one. It may seem that now the suitability of function F to discriminate F/NF behaviors is perfect; however, it is worth noting that the sample is quite small (there is only one event in the right circle), so the success of the adjustment arises partly from a favorable combination of circumstances.

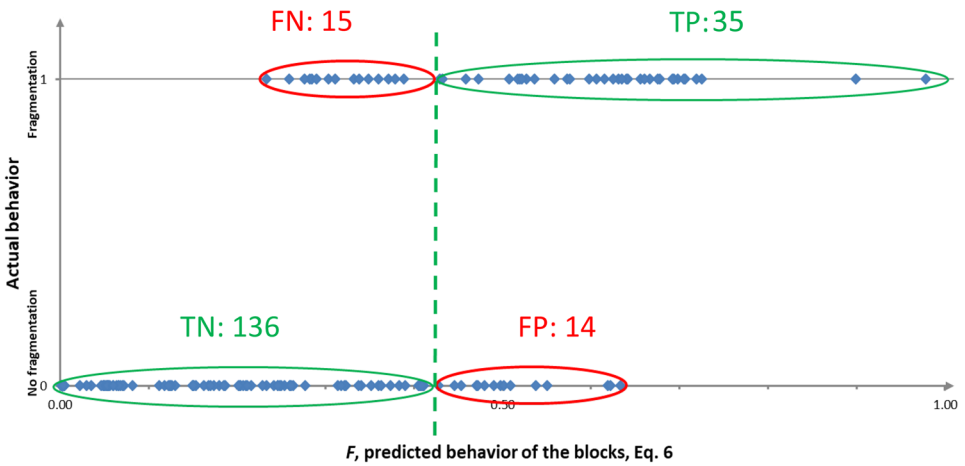

Fig. 17 Function F (Eq. 6) adjusted for the 200 impact events, test 1–4. The actual behavior (vertical axis) equals 1 in case of significant fragmentation or 0 in case of no fragmentation, according to last column in Tables 1–4. The colored ellipses enclose the true negatives (TN), true positives (TP), false negatives (FN), and false positives (FP), being the corresponding figure the number of cases inside

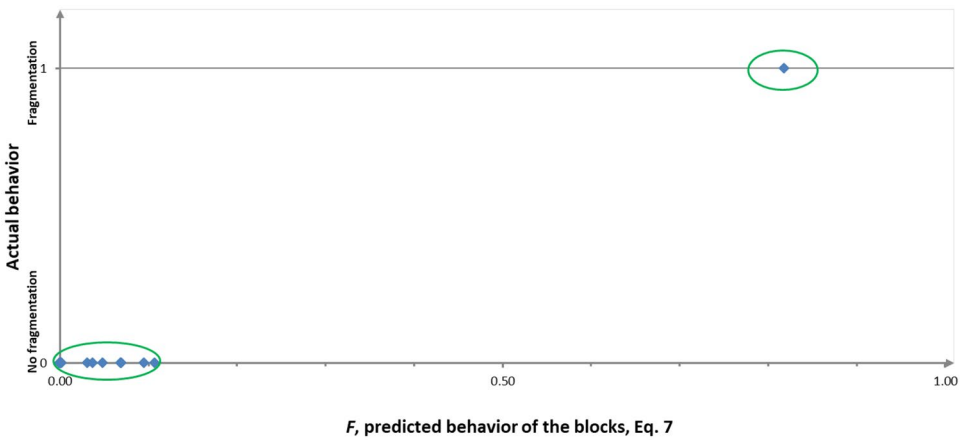

Fig. 18 Function F (Eq. 7) adjusted for a subset of 30 impact events, test 3. The actual behavior (vertical axis) equals 1 in case of significant fragmentation or 0 in case of no fragmentation, according to last column in Table 3. Note that 22 points fall close to the origin

Conclusions

In this paper we have presented four field tests carried out in quarries with the aim of improving knowledge of the rockfall process, with a special emphasis on the eventual fragmentation of the blocks on impact with the slope.

The design of the tests has been outlined, with some details on the setup and technical equipment (cameras and video recording, drone, personnel and machinery) as well as on the procedure. During the four tests, spanning more than 3 years, there was an evolution in the setup, with improvements in efficiency and safety. New available tools, such as drones, high-speed video cameras, and last generation digital photogrammetric software, were progressively introduced and proved to be very useful for block trajectometry and volumetry. The 3 HS&HR video cameras permitted the derivation of important 3D data (velocities and incidence angles, for instance), which are of paramount importance for energy considerations. The added value of all the image acquisition was the reviewing of the drops (slow motion, multi-angle), and the possibility of extracting values or features not envisaged at the beginning (i.e., the substrate type at the impact point, the relative attitude block/ground, and the overall performance of the block in relation to the fragmentation). However, for post-processing all the raw material, the second, third, and fifth author have had to develop several pieces of new ad hoc software. This task will continue until the completion of the GeoRisk project.

The information gathered or computed is summarized in Tables 1–4 (124 blocks, 200 impact events), including as much as 11 values per event. An overall result for the four tests is that almost 40% of all blocks were "significantly" broken during the launch (54% of the limestone blocks; 14% of the granitoids). However, all these figures are completely site-dependent.

In relation with the angle of aperture occupied by the fragments just after the block breakage (θ angle in Fig. 14), we delimit the value in the range 25°–145°. On the other hand, the size distributions of the fragments after the breakages have been carefully studied in Ruiz-Carulla et al. (2020). It has been confirmed that the power law adjusts quite well with the cumulative fragment size distribution for the four tests, with negative *exponents* between 0.31 and 0.54. These values (θ angle and BSD *exponent*) will be very useful within propagation models that include the eventual fragmentation of the initial mass.

We have discussed the different factors that may affect the behavior of the blocks during the drops, working out why some of the blocks break, while others remain almost intact. Instead of trying to identify an energy threshold explaining the breakage/non-breakage of the different blocks, we have classified other influencing variables like the incidence angle, the substrate where the block impacts, the contact geometry and the block lithology. Everything has been combined together into a function, F (Eq. 5), which aims to model or explain the overall block performance in terms of fragmentation/no fragmentation. A least square approach was used to adjust the exponents of the different terms of the function. Finally, an incipient result was obtained (Fig. 17) which discriminates quite satisfactorily (in the "break/no-break" aspect) the set of results of the 124 blocks released in the four tests. Although F misclassifies some blocks, it has the merit of considering, simultaneously, the different actors in the phenomena, in particular the *Specific Normal Energy*, the substrate and the relative attitude block/ground. The function is not intended to be of general application, as it is very site- and setup-dependent; it is only a humble proposal, a small step forward, requiring more work to confirm its real applicability.

Acknowledgements

The authors acknowledge the support of the Spanish Ministry of Economy and Competitiveness for the research projects RockRisk (BIA2013-42582-P), RockModels (BIA2016-75668-P, AEI, ERDF/FEDER, UE) and GeoRisk (PID2019-103974RB-I00/AEI/10.13039/501100011033). GeoRisk is funded by the Agencia Estatal de Investigación (AEI) on the framework of the Plan for Scientific-Technical Research and Innovation. The support of the Spanish Ministry of Education (grants to the second and third authors, codes FPU13/04252 and BES-2014-069795, respectively) and the BBVA Foundation (thirteenth author's contract) is also appreciated. The collaboration of Canteras Hermanos Foj and Canteras Ponderosa S.A., Marc Janeras, and S. Moreno is greatly acknowledged. Finally, we thank two anonymous reviewers and the Editor who helped to improve the structure and content of the final version.

Funding

Open Access funding provided thanks to the CRUE-CSIC agreement with Springer Nature.

Availability of data and material

The numerical data used in this work and a significant sample of graphical information are included in the Electronic Supplementary Material as specified in the different sections of the paper. Some additional data can be found at the RockModels project web repository (rockmodels.upc.edu/en); in case of any specific query, send a message through its contact mailbox.

Declarations

Conflict of interest The authors declare no competing interests.

References

Abellán A, Vilaplana JM, Martinez J (2006) Application of a long-range terrestrial laser scanner to a detailed rockfall study at Vall de Nuria (Eastern Pyrenees, Spain). Eng Geology 88:136–148. https://doi.org/10.1016/j.enggeo.2006.09.012

Agliardi F, Crosta GB (2003) High resolution three-dimensional numerical modelling of rockfalls. Int J Rock Mech Min Sci 40:455–471. https://doi.org/10.1016/S1365-1609(03)00021-2
Agliardi F, Crosta GB, Frattini P (2009) Integrating rockfall risk assessment and countermeasure design by 3D modelling techniques. Nat Hazards Earth Syst Sci 9:1059–1073. https://doi.org/10.5194/nhess-9-1059-2009
Asteriou P, Saroglou H, Tsiambaos G (2012) Geotechnical and kinematic parameters affecting the coefficients of restitution for rock fall analysis. Int J Rock Mech Min 54:103–113. https://doi.org/10.1016/j.ijrmms.2012.05.029
Asteriou P, Tsiambaos G (2016) Empirical model for predicting rockfall Trajectory Direction. Rock Mech Rock Eng 49:927–941. https://doi.org/10.1007/s00603-015-0798-7
Asteriou P, Tsiambaos G (2018) Effect of impact velocity, block mass and hardness on the coefficients of restitution for rockfall analysis. Int J Rock Mech Min Sci 106:41–50. https://doi.org/10.1016/j.ijrmms.2018.04.001
Azimi C, Desvarreux P, Giraud A, Martin-Cocher J (1982) Méthode de calcul de la dynamique des chutes de blocs-Application à l'étude du versant de la montagne de La Pale (Vercors). Bull. Liaison Labor. P. et Ch., vol. 122. pp 93–102
Azzoni A, de Freitas MH (1995) Experimentally gained parameters, decisive for rock fall analysis. Rock Mech Rock Engng 28:111–124. https://doi.org/10.1007/BF01020064
Barton N, Lien R, Lunde J (1974) Engineering classification of rock masses for the design of tunnel support. Rock Mech 6:189–236. https://doi.org/10.1007/BF01239496
Bieniawski ZT (1993) Classification of rock masses for engineering: the RMR system and future trends. In: Hudson JN (ed) Rock Testing and Site Characterization. Pergamon Press, Oxford (UK), pp 553–573
Bourrier F, Dorren L, Hungr O (2013) The use of ballistic trajectory and granular flow models in predicting rockfall propagation. Earth Surf Processes Landforms 38:435–440. https://doi.org/10.1002/esp.3372
Bourrier F, Toe D, Garcia B, Baroth J, Lambert S (2021) Experimental investigations on complex block propagation for the assessment of propagation models quality. Landslides 18:639–654. https://doi.org/10.1007/s10346-020-01469-5
Caviezel A, Christen M, Bühler Y, Bartelt P (2017) Calibration methods for numerical rockfall models based on experimental data. Proceedings of ROCEXS 2017, 6th Interdisciplinary Workshop on Rockfall Protection, May 2017, Barcelona (Spain). pp 59–62. Available at: http://congress.cimne.com/rocexs2017/frontal/Doc/Ebook.pdf. Accessed 20 January 2020
Caviezel A, Demmel SE, Ringenbach A, Bühler Y, Lu G, Christen M, Dinneen CE, Eberhard LA, von Rickenbach D, Bartelt P (2019) Reconstruction of four-dimensional rockfall trajectories using remote sensing and rock-based accelerometers and gyroscopes. Earth Surf Dyn 7:199–210. https://doi.org/10.5194/esurf-7-199-2019
Charrière M, Humair F, Froese C, Jaboyedoff M, Pedrazzini A, Longchamp C (2015) From the source area to the deposit: collapse, fragmentation, and propagation of the Frank Slide. GSA Bull 128:332–351. https://doi.org/10.1130/B31243.1
Chau KT, Wong RHC, Wub JJ (2002) Coefficient of restitution and rotational motions of rockfall impacts. Int J Rock Mech Min Sci 39:69–77. https://doi.org/10.1016/S1365-1609(02)00016-3
Coombs S, Apostolov A, Take A, Benoit J (2018) Quantifying the significance of collisional flow on the mobility of dry granular landslides using a Smart Rock sensor. In: EGU General Assembly Conference Abstracts, vol. 20. p 9450.
Corominas J, Copons R, Moya J, Vilaplana JM, Altimir J, Amigó J (2005) Quantitative assessment of the residual risk in a rock fall protected area. Landslides 2(4):343–357. https://doi.org/10.1007/s10346-005-0022-z
Corominas J, Matas G, Ruiz-Carulla R (2019) Quantitative analysis of risk from fragmental rockfalls. Landslides 16:5–21. https://doi.org/10.1007/s10346-018-1087-9
Corominas J, Mavrouli O (2011) Rockfall quantitative risk assessment, Chapter 8. In: Lambert S, Nicot F (eds) Rockfall Engineering. ISTE Ltd & John Wiley and Sons, Inc., London (UK), pp 255–301
Corominas J, Mavrouli O, Santana D, Moya J (2012) Simplified approach for obtaining the block volume distribution of fragmental rockfalls. Proceed XI International Symposium on Landslides, Banff (Canada). In: Eberhardt et al. (Eds) Landslides and engineered slopes. Taylor & Francis Group. pp 1159–1164.
Corominas J, Mavrouli O, Ruiz-Carulla R (2017a) Rockfall occurrence and fragmentation. In: Sassa K, Mikoš M, Yin Y (Eds): Advancing Culture of Living with Landslides. World Landslide Forum, WLF 2017, Ljubljana. Springer, Cham. pp 75–97. https://doi.org/10.1007/978-3-319-59469-9_4
Corominas J, Lantada N, Gili J, Ruiz R, Matas G, Mavrouli O, Núñez-Andrés MA, Moya J, Buill F, Abellán A, Puig-Polo C, Prades A, Martinez-Bofill J, Salo L (2017b) The RockRisk project: rockfall risk quantification and prevention. Proceedings of ROCEXS 2017, 6th Interdisciplinary Workshop on Rockfall Protection, May 2017, Barcelona (Spain). pp 39–42. Available at: http://congress.cimne.com/rocexs2017/frontal/Doc/Ebook.pdf. Accessed 20 January 2020
Corominas J, Mavrouli O, Ruiz-Carulla R (2018) Magnitude and frequency relations: are there geological constraints to the rockfall size? Landslides 15(5):829–845. https://doi.org/10.1007/s10346-017-0910-z
Cruden DM, Varnes DJ (1996) Landslides: investigation and mitigation. Special Report 247. Transportation Research Board, US National Research Council. Chapter Landslides Types and Processes. pp 36–75. Available at: http://onlinepubs.trb.org/Onlinepubs/sr/sr247/sr247-003.pdf. Accessed 20 January 2020
Dorren LKA, Berger F, Putters US (2006) Real-size experiments and 3-D simulation of rockfall on forested and non-forested slopes. Nat Haz Earth Sys Sci 6:145–153. https://doi.org/10.5194/nhess-6-145-2006
Duffy J, Glover J (2017) A brief history of rockfall barrier testing. Proceedings of ROCEXS 2017, 6th Interdisciplinary Workshop on Rockfall Protection, May 2017, Barcelona (Spain). pp 115–121. Available at: http://congress.cimne.com/rocexs2017/frontal/Doc/Ebook.pdf. Accessed 20 January 2020
Dussauge C, Grasso JR, Helmstetter A (2003) Statistical analysis of rockfall volume distributions: implications for rockfall dynamics. Journal of Geophysical Research: Solid Earth, AGU 108(B6):2286. https://doi.org/10.1029/2001JB000650
Evans SG, Hungr O (1993) The assessment of rockfall hazard at the base of talus slopes. Can Geotech J 30:620–636. https://doi.org/10.1139/t93-054
Falcetta JL (1985) Un nouveau modèle de calcul de trajectoires de blocs rocheux. Rev Fr Géotech 30:11–17. https://doi.org/10.1051/geotech/1985030011
Fell R, Ho KKS, Lacasse S, Leroi E (2005) A framework for landslide risk assessment and management. In: Hungr O, Fell R, Couture R, Eberthardt E (eds) Landslide Risk Management. Taylor and Francis, London (UK), pp 3–25
Ferrari F, Giacomini A, Thoeni K (2016) Qualitative rockfall hazard assessment: a comprehensive review of current practices. Rock Mech Rock Eng 49:2865–2922. https://doi.org/10.1007/s00603-016-0918-z
Gerber W, Grassl H, Böll A, Ammann W (2001) Flexible rockfall barriers – development, standardisation and type-testing in switzerland. in: international conference on landslides - causes, impacts and countermeasures, 17–21 June 2001, Davos (Switzerland). Kuehne M, Einstein HH, Krauter E, Klapperich H, Poettler R (eds), Verlag Glueckauf Gmbh, Essen (Germany). ISBN 3–7739–5969–9: pp 515–524
Gerber W, Caviezel A (2017) Diversity of the results from drop weight tests. Proceedings of ROCEXS 2017, 6th Interdisciplinary Workshop on Rockfall Protection, May 2017, Barcelona (Spain). pp 63–66. Available at: http://congress.cimne.com/rocexs2017/frontal/Doc/Ebook.pdf. Accessed 20 January 2020
Giacomini A, Buzzi O, Renard B, Giani GP (2009) Experimental studies on fragmentation of rock falls on impact with rock surfaces. Int J Rock Mech Min Sci 46:708–715. https://doi.org/10.1016/j.ijrmms.2008.09.007
Giacomini A, Thoeni K, Lambert C, Booth S, Sloan SW (2012) Experimental study on rockfall drapery systems for open pit highwalls. Int J Rock Mech Min Sci 56:171–181. https://doi.org/10.1016/j.ijrmms.2012.07.030
Gili JA, Ruiz-Carulla R, Matas G, Corominas J, Lantada N, Núñez MA, Mavrouli O, Buill F, Moya J, Prades A, Moreno S (2016) Experimental study on rockfall

fragmentation: in situ test design and firsts results. Proceed. 12th Int Symp on Landslides (ISL 2016), Napoli (Italy). In: Aversa S, Cascini L, Picarelli L, Scavia C (eds) Landslides and engineered slopes, vol. 2. pp 983–990. https://doi.org/10.1201/9781315375007

Haug ØT, Rosenau M, Leever K, Oncken O (2016) On the energy budgets of fragmenting rockfalls and rockslides: insights from experiments. J Geophys Res Earth Surface 121:1310–1327. https://doi.org/10.1002/2014JF003406

Hibert C, Talib M, Noël F, Gracchi T, Bourrier F, Brenguier O, Desrues M, Toe D, Wyser E, Malet JP, Jaboyedoff M (2019) Analysis of the dynamics of supervised single-block rockfalls from intra-block accelerometers, seismology and remote sensing. Geophys Res Abstr 21:1–1

Hoek E (2006) Practical rock engineering, 2006 edn, Chapter 9. p 1. https://www.rocscience.com/assets/resources/learning/hoek/Practical-Rock-Engineering-Full-Text.pdf Accessed 20 January 2020

Hungr O, Evans SG, Hazzard J (1999) Magnitude and frequency of rock falls along the main transportation corridors of southwestern British Columbia. Can Geotech J 36:224–238. https://doi.org/10.1139/t98-106

Hungr O, Corominas J, Eberhardt E (2005) Estimating landslide motion mechanisms, travel distance and velocity. In: Hungr O, Fell R, Couture R, Eberthardt E (eds) Landslide Risk Management. Taylor and Francis, London, pp 99–128

Hungr O, Leroueil S, Picarelli L (2014) The Varnes classification of landslide types, an update. Landslides 11(2):167–194. https://doi.org/10.1007/s10346-013-0436-y

Jaboyedoff M, Dudt JP, Labiouse V (2005) An attempt to refine rockfall hazard zoning based on the kinetic energy, frequency and fragmentation degree. Nat Haz Earth Syst Sci 5:621–632. https://doi.org/10.5194/nhess-5-621-2005

James MR, Robson S (2012) Straightforward reconstruction of 3D surfaces and topography with a camera: accuracy and geoscience application. J Geophys Res 117:F03017. https://doi.org/10.1029/2011JF002289

Labiouse V, Heidenreich B (2009) Half-scale experimental study of rockfall impacts on sandy slopes. Nat Hazards Earth Syst Sci 9:1981–1993. https://doi.org/10.5194/nhess-9-1981-2009

Li L, Lan H (2015) Probabilistic modeling of rockfall trajectories: a review. Bull Eng Geol Environ 74:1163–1176. https://doi.org/10.1007/s10064-015-0718-9

Lisjak A, Spadari M, Giacomini A, Grasselli G (2010) Rock fall numerical modelling using a combined finite-discrete element approach. Proceedings Symp. Rock Slope Stability, November 2010, Paris (France).

Marinos P, Hoek E (2000) GSI: a geologically friendly tool for rock mass strength estimation. In: Proceed. ISRM Int. Symp. Pub. Int. Soc. for Rock Mech. and Rock Eng. CRC Press. Available at: https://www.academia.edu/download/38008118/H2000a.pdf. Accessed 20 January 2020

Matas G, Lantada N, Corominas J, Gili JA, Ruiz-Carulla R, Prades A (2017) RockGIS: a GIS-based model for the analysis of fragmentation in rockfalls. Landslides 14:1565–1578. https://doi.org/10.1007/s10346-017-0818-7

Matas G, Lantada N, Corominas J, Gili JA, Ruiz-Carulla R, Prades A (2020) Simulation of full-scale rockfall tests with a fragmentation model. Geosciences, Section "Natural Hazards". In: Hantz D, Jaboyedoff M (eds) Special Issue on Rock Fall Hazard and Risk Assessment, vol. 10. p 168. https://doi.org/10.3390/geosciences10050168

Matthews JA, Winkler S, Wilson P, Tomkins MD, Dortch JM, Mourne RW, Hill JL, Owen G, Vater AE (2018) Small rock-slope failures conditioned by Holocene permafrost degradation: a new approach and conceptual model based on Schmidt-hammer exposure-age dating, Jotunheimen, southern Norway. Boreas 47:1144–1169. https://doi.org/10.1111/bor.12336

Moradian ZA, Behnia M (2009) Predicting the uniaxial compressive strength and static young's modulus of intact sedimentary rocks using the ultrasonic test. ASCE Int J Geomech 9. https://doi.org/10.1061/(ASCE)1532-3641(2009)9:1(14)

Noël F, Wyser E, Jaboyedoff M, Hibert C, Talib M, Malet JP, Toussaint R, Desrues M, Bourrier F, Toe D, Brenguier O, Gracchi T, Derron MH, Cloutier C, Locat J (2019) Real-size rockfall experiment: applying observed impact dynamics to 3D rockfall simulations on highly detailed terrain models. Geophys. Res. Abstr. 21:p1–1. 1p

Prades A, Matas G, Núñez-Andrés MA, Buill F, Lantada N, Corominas J (2017) Determinación de trayectorias de bloques rocosos en ensayos mediante videogrametría. Proceed. Primer Congreso en Ingeniería Geomática, Universitat Politècnica de València. pp 34–40. http://dx.doi.org/10.4995/CIGeo2017.2017.6617

Ritchie AM (1963) The evaluation of rockfall and its control, Highway Research Record 17, Highway Research Board, National Research Council, Washington DC (USA). pp 13–28. Available at: http://onlinepubs.trb.org/Onlinepubs/hrr/1963/17/17-002.pdf. Accessed 20 January 2020

Romana M, Serón JB, Montalar E (2003) SMR geomechanics classification: application, experience and validation. In: Proceed. 10th ISRM Congress. Pub. Int. Soc. for Rock Mech. and Rock Eng & South African Inst Min Metall. Available at: https://www.academia.edu/download/31693316/SMR_geomechanics_classification_for_ICRM_2003.pdf. Accessed 20 January 2020

Ruiz-Carulla R, Corominas J, Mavrouli O (2015) A methodology to obtain the block size distribution of fragmental rockfall deposits. Landslides 12:815–825. https://doi.org/10.1007/s10346-015-0600-7

Ruiz-Carulla R, Corominas J, Mavrouli O (2016a) Comparison of block size distribution in rockfalls. Proceed. 12th Int Symp on Landslides (ISL 2016), Napoli (Italy). In: Aversa S, Cascini L, Picarelli L, Scavia C (eds) Landslides and engineered slopes, vol. 3. pp 1767–1774. https://doi.org/10.1201/9781315375007

Ruiz-Carulla R, Matas G, Prades A, Gili JA, Corominas J, Lantada N, Buill F, Mavrouli O, Núñez MA, Moya J (2016b) Analysis of rock block fragmentation by means of real-scale tests. Proceed. 3rd RSS, Rock Slope Stability conference, Lyon (France). pp 107–108

Ruiz-Carulla R, Corominas J, Mavrouli O (2017) A fractal fragmentation model for rockfalls. Landslides 14:875–889. https://doi.org/10.1007/s10346-016-0773-8

Ruiz-Carulla R (2018) Rockfall analysis: failure, fragmentation and propagation characterization. A fractal fragmentation of rockfalls. Ph.D Thesis, Technical University of Catalonia. Department of Civil and Environmental Engineering. pp 354. Available at: http://hdl.handle.net/2117/121044. Accessed 20 January 2020

Ruiz-Carulla R, Corominas J (2019) Analysis of rockfalls by means of a fractal fragmentation model. Rock Mech Rock Eng 1–23.https://doi.org/10.1007/s00603-019-01987-2

Ruiz-Carulla R, Corominas J, Gili JA, Matas G, Lantada N, Moya J, Prades A, Núñez-Andrés MA, Buill F (2020) Puig C (2020) Analysis of fragmentation of rock blocks from real-scale tests. Geosciences 10:308. https://doi.org/10.3390/geosciences10080308

Saló L, Corominas J, Lantada N, Matas G, Prades A, Ruiz-Carulla R (2018) Seismic energy analysis as generated by impact and fragmentation of single-block experimental rockfalls. J Geophys Res Earth Surface 123:1450–1478. https://doi.org/10.1029/2017JF004374

Santana D, Corominas J, Mavrouli O, Garcia-Sellés D (2012) Magnitude-frequency relation for rockfall scars using a Terrestrial Laser Scanner. Eng Geology 145:50–64. https://doi.org/10.1016/j.enggeo.2012.07.001

Scavia C, Barbero M, Castelli M, Marchelli M, Peila D, Torsello G, Vallero G (2020) Evaluating rockfall risk: some critical aspects. Geosciences vol. 10. pp 98. https://doi.org/10.3390/geosciences10030098

Spadari M, Giacomini A, Buzzi O, Fityus S, Giani GP (2012) In situ rockfall testing in New South Wales. Australia, Int J Rock Mech Min Sci 49:84–93. https://doi.org/10.1016/j.ijrmms.2011.11.013

Turner AK, Jayaprakash GP (2012) Introduction. In Turner AK, Schuster RL (eds) Rockfall characterization and control. Transportation Research Board, National Academy of Sciences. Washington DC (USA), ISBN 0309223121. pp 3–20

Volkwein A, Schellenberg K, Labiouse V, Agliardi F, Berger F, Bourrier F, Dorren LKA, Gerber W, Jaboyedoff M (2011) Rockfall characterisation and structural protection – a review. Nat Haz Earth Syst Sci 11:2617–2651. https://doi.org/10.5194/nhess-11-2617-2011

Volkwein A, Kummer P, Sutter T (2017) Fully recorded rockfall trajectories. In: Proceedings of ROCEXS 2017, 6th Interdisciplinary Workshop on Rockfall Protection, May 2017, Barcelona (Spain). pp 122–125. Available at: http://congress.cimne.com/rocexs2017/frontal/Doc/Ebook.pdf. Accessed 20 January 2020

Wang Y, Tonon F (2011) Discrete element modeling of rock fragmentation upon impact in rock fall analysis. Rock Mech Rock Eng 44:23–35. https://doi.org/10.1007/s00603-010-0110-9

Yasar E, Erdogan Y (2004) Correlating sound velocity with the density, compressive strength and Young's modulus of carbonate rocks. Int J Rock Mech Min Sci 41:871–875. https://doi.org/10.1016/j.ijrmms.2004.01.012

Zhang ZX, Kou SQ, Jiang LG, Lindqvist PA (2000) Effects of loading rate on rock fracture: fracture characteristics and energy partitioning. Int J Rock Mech Min Sci 37:745–762. https://doi.org/10.1016/S1365-1609(00)00008-3

Zhao T, Dai F, Crosta GB, De Blasio F, Utili S (2016) DEM simulations of simple fragmentation experiments. Proceed. 12th Int Symp on Landslides (ISL 2016), Napoli (Italy). In: Aversa S, Cascini L, Picarelli L, Scavia C (eds) Landslides and engineered slopes, vol. 3. pp 2113–2119. https://doi.org/10.1201/9781315375007

Zhou S, Ouyang C, An H, Jiang T, Xu Q (2020) Comprehensive study of the Beijing Daanshan rockslide based on real-time videos, field investigations, and numerical modeling. Landslides 17:1217–1231. https://doi.org/10.1007/s10346-020-01345-2

Supplementary Information The online version contains supplementary material available at https://doi.org/10.1007/s10346-021-01837-9.

J. A. Gili (✉) · R. Ruiz-Carulla · G. Matas · J. Moya · A. Prades · J. Corominas · N. Lantada · M. A. Núñez-Andrés · F. Buill · C. Puig · J. Martínez-Bofill
Department of Civil and Environmental Engineering (DECA), Division of Geotechnical Engineering and Geosciences, Universitat Politècnica de Catalunya (UPC), Barcelona, Spain
Email: j.gili@upc.edu

Ll. Saló
Department of Civil and Environmental Engineering, Massachusetts Institute of Technology, Cambridge, MA, USA

O. Mavrouli
University of Twente, Enschede, The Netherlands